# Synchronizing chaos in an experimental chaotic pendulum using methods from linear control theory

Sander Kaart, Jaap C. Schouten,* and Cor M. van den Bleek
*Department of Chemical Process Technology, Delft University of Technology, Julianalaan 136, 2628 BL Delft, The Netherlands*
(Received 16 September 1998)

Linear feedback control, specifically model predictive control (MPC), was used successfully to synchronize an experimental chaotic pendulum both on unstable periodic and aperiodic orbits. MPC enables tuning of the controller to give an optimal controller performance. That is, both the fluctuations around the target trajectory and the necessary control actions are minimized using a least-squares solution of the linearized problem. It is thus shown that linear control methods can be applied to experimental chaotic systems, as long as an adequate model is available that can be linearized along the desired trajectory. This model is used as an observer, i.e., it is synchronized with the experimental pendulum to estimate the state of the experimental pendulum. In contrast with other chaos control procedures like the map-based Ott, Grebogi, and York method [Phys. Rev. Lett. **64**, 1196 (1990)], the continuous type feedback control proposed by Pyragas [Phys. Lett. A **170**, 421 (1992)], or the feedback control method recently proposed by Brown and Rulkov [Chaos **7** (3), 395 (1997)], the procedure outlined in this paper automatically results in a choice for the feedback gains that gives optimum performance, i.e., minimum fluctuations around the desired trajectory using minimum control actions.
[S1063-651X(99)09505-7]

PACS number(s): 05.45.−a

## I. INTRODUCTION

Chaos control is a vast expanding field of research with many applications in, e.g., secure communications [1,2], electronics [3,4], mechanical engineering [5–9], and fluidization engineering [10–12]. Many chaos control methods have been proposed in the past decade, see e.g., Chen and Dong [13], Rulkov [3], Shinbrot [14], and Kapitaniak [15] for reviews on the subject. A number of these control methods can be used only in specific cases like, e.g., control by the construction of Lyapunov functions, or are sensitive to noise, like the OGY method [16].

In this paper, a *general* control method for chaotic systems is proposed, based on *linear* control theory [17,18]. The practical implementation of this linear control method will be illustrated by the control of an experimental driven damped chaotic pendulum. To apply linear control methods to a nonlinear system, it is linearized along some nominal trajectory, as is usual practice in classic linear control theory [18]. Here the system is linearized along the desired unstable periodic orbit (UPO) or aperiodic orbit (AO), in a similar way as has been recently proposed by Brown and Rulkov [19].

The control methods described in this paper are all based on full state feedback control [17], for which the full state of the pendulum has to be known (i.e., angular displacement, angular velocity, and drive phase). However, the pendulum used here only allows its angular displacement to be measured [8,9]. For that reason the full state of the pendulum will be estimated by using an observer. An observer is a model that is synchronized with the experimental system. After synchronization, the observer's state will be the same as the experimental system's state. The full state feedback procedure is sketched in Fig. 1.

When using (full state) feedback control, a choice for the feedback gain matrix **K** has to be made. In this paper two methods are used for choosing **K** and each method is implemented in two different ways. The first method stabilizes the unstable poles of the system by choosing appropriate feedback gains and will be referred to as the *pole-placement*

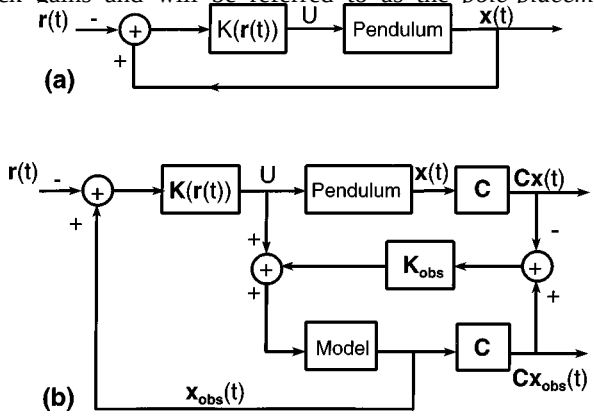


FIG. 1. (a) Full state feedback control scheme. The difference between the reference state $\mathbf{r}(t)$ and the dynamical system's state $\mathbf{x}(t)$ is used to compute the control input $u$ by multiplying this difference with the feedback gain matrix **K**. (b) If the full state of the dynamical system cannot be measured, it can be estimated using an observer. An observer is a model that is synchronized with the experimental system, using the difference between the measured state variables $\mathbf{Cx}(t)$ and simulated state variables $\mathbf{Cx}_{\mathrm{obs}}(t)$. Here **C** is the observation matrix that isolates the measured state variable from the full state. For the experimental pendulum only the angular displacement of the pendulum can be measured, so $\mathbf{Cx}(t)=\theta(t)$. The observer gain matrix $\mathbf{K}_{\mathrm{obs}}$ is used to synchronize the observer with the experimental system.

*Present address: Laboratory of Chemical Reactor Engineering, Eindhoven University of Technology, P.O. Box 513, 5600 MB Eindhoven, The Netherlands.

 ©1999 The American Physical Society

method in the remainder of this paper. This technique is further described in Sec. II A 1.

Usually it is not straightforward to choose feedback gains in such a way that both the deviations from the target trajectory *and* the control actions become sufficiently small. The second method for choosing **K** finds an optimum solution for this problem and will from now on be referred to as the *optimal-control* method. Optimal control is implemented in two ways as will be discussed in Sec. II A 2.

The design of the observer is discussed in Sec. II B. In Sec. III the results of the two control methods will be illustrated by four different implementations. Finally, in Sec. IV the conclusions will be presented.

## II. THEORY

This section presents the methods used to synchronize the experimental chaotic pendulum with target trajectories that are embedded in the pendulum's chaotic attractor. These target trajectories are UPO's and AO's. Examples of AO's are previously measured time series of the state of the pendulum $(\mathbf{x}(t))$ or the chaotic trajectory of another (but dynamically identical) pendulum. The theory is applicable to both stabilizing UPO's and synchronizing two AO's since stabilization and synchronization of chaotic systems are similar phenomena. In both cases the response system, i.e., the system that has to be controlled, has to follow a (imaginary) driving system that moves on a desired trajectory.

Let us consider the following driving system:

$$\dot{\mathbf{r}}(t)=\mathbf{F}(\mathbf{r}(t),t), \tag{1}$$

where the desired trajectory is represented by vector $\mathbf{r}(t)$, which is the system's state. Function **F** is a vector-valued function. The dynamics of the response system become

$$\dot{\mathbf{x}}(t)=\mathbf{F}(\mathbf{x}(t),t)+\mathbf{E}(\mathbf{x}(t)-r(t)), \tag{2}$$

where **E** is a vector-valued function and represents the coupling between the driving and response systems. When both systems are synchronized, hence $\mathbf{x}(t)=\mathbf{r}(t)$, the coupling between both systems becomes zero, or $\mathbf{E}=0$. The motion around the target trajectory $\mathbf{r}(t)$ can be represented by a linearization along this target trajectory,

$$\delta\dot{\mathbf{r}}(t)=[\mathbf{DF_r}(\mathbf{r}(t),t)+\mathbf{DE_r}(\mathbf{r}(t))]\,\delta\mathbf{r}(t), \tag{3}$$

Here $\delta\mathbf{r}(t)$ is the deviation from the target trajectory $\mathbf{r}(t)$, and $\mathbf{DF_r}$ and $\mathbf{DE_r}$ are the Jacobians of **F** and **E**, evaluated along $\mathbf{r}(t)$. By substitution of $\mathbf{A}=\mathbf{DF}_r$ and $-\mathbf{K}=\mathbf{DE}_r$, this equation can be written in a different, more familiar form as

$$\dot{\mathbf{e}}(t)=[\mathbf{A}(\mathbf{r}(t),t)-\mathbf{K}(\mathbf{r}(t))]\mathbf{e}(t), \tag{4}$$

where $\mathbf{e}(t)=\mathbf{x}(t)-\mathbf{r}(t)$, i.e., the deviation from the desired trajectory. Now we have to find the appropriate coupling gain matrix **K** that will synchronize the response system with the drive system, i.e., $\|\mathbf{e}(t)\|\to 0$ if $t\to\infty$. In linear control theory, Eq. (4) is usually considered as the closed-loop response of a full state feedback controlled system. How to determine the appropriate coupling gain, or feedback matrix **K** is the subject of Sec. II A.

### A. Full state feedback control

The experimental driven damped pendulum can be adequately described by the following set of ODE's [21], and Eq. (1) thus becomes

$$\dot{\mathbf{r}}(t)=\mathbf{F}(\mathbf{r}(t),t)=\begin{cases}\dfrac{d\omega}{dt}=-p_1\omega-p_2\sin(\theta)+p_3\sin(\phi),\\ \dfrac{d\theta}{dt}=\omega,\\ \dfrac{d\phi}{dt}=\omega_D.\end{cases} \tag{5}$$

Here $p_1$, $p_2$, and $p_3$ are constants related to friction, gravity, and the driving force, respectively. The angular velocity ($\omega$), the angular displacement ($\theta$), and the drive phase ($\phi$) together represent the pendulum's full state $\mathbf{r}(t)=[\omega(t)\,\theta(t)\,\phi(t)]^T$. The Jacobian, **DF** of the set of ODE's in Eq. (5), becomes

$$\mathbf{DF}=\begin{pmatrix}-p_1 & -p_2\cos(\theta_r(t)) & +p_3\cos(\phi_r(t))\\ 1 & 0 & 0\\ 0 & 0 & 0\end{pmatrix}, \tag{6}$$

where $\theta_r(t)$ and $\phi_r(t)$ denote the angular displacement and drive phase corresponding to the target trajectory $\mathbf{r}(t)$. For the experimental chaotic pendulum, the drive phase of the response system $\phi(t)$ always equals the drive phase of the drive system $\phi_r(t)$. This means that the dynamics of relevance are described by the following Jacobian,

$$\mathbf{DF}=\begin{pmatrix}-p_1 & -p_2\cos(\theta_r(t))\\ 1 & 0\end{pmatrix}, \tag{7}$$

Now the deviation $\mathbf{e}(t)$ from the target trajectory $\mathbf{r}(t)$ is described by

$$\dot{\mathbf{e}}(t)=\left[\begin{pmatrix}-p_1 & -p_2\cos(\theta_r(t))\\ 1 & 0\end{pmatrix}-\begin{pmatrix}k_{c,1} & k_{c,2}\\ 0 & 0\end{pmatrix}\right]\cdot\mathbf{e}(t), \tag{8}$$

where $k_{c,1}$ and $k_{c,2}$ are the nonzero elements of the feedback matrix $\mathbf{K}_c$. The second row of $\mathbf{K}_c$ will contain zeros, since there is no way of directly changing the angular displacement. The pendulum can only be controlled by applying an extra force on it.

An intuitive approach of choosing $\mathbf{K}_c$ in Eq. (8) is to make sure the poles of the system lie in the left half-plane. If the system described by Eq. (8) would be time invariant, choosing the poles in the left half-plane would yield the desired synchronization. Since the system is not time invariant, negative real parts of the poles do not guarantee successful synchronization [19]. However, if the poles are placed sufficiently far away from the imaginary axis, synchronization will occur. Hence, this intuitive approach will be used to find an estimate for $\mathbf{K}_c$. Through a rigorous linear stability analysis, Brown and Rulkov [19] derived a sufficient condition to place the poles of systems with time-dependent parameters, like Eq. (8), sufficiently far into the left half-plane. For Eq. (8), the intuitive condition satisfies the rigorous condition derived by Brown and Rulkov [19]. In general, this does not

have to be the case. However, since the rigorous condition is only sufficient and not necessary, the intuitive approach can be used to give an initial guess for $\mathbf{K}_c$. Although this linear stability analysis promises stable synchronous motion, noise and nonlinear effects, like e.g., the bubbling of attractors [20] may prevent long-term stable synchronous motion. Two possible ways of choosing the location of the poles are discussed in the Sec. II A 1.

#### *1. Pole placement*

The poles of Eq. (8) are

$$\lambda_{1,2}=-\frac{1}{2}(p_1+k_{c,1}) \pm\frac{1}{2}\sqrt{(p_1+k_{c,1})^{\theta}-4[p_2\cos(\theta_r(t))+k_{c,2}]}. \quad (9)$$

To keep the real parts of these poles in the left half of the complex plane, the conditions $k_{c,1}>-p_1$ and $k_{c,2}>-p_2\cos(\theta_r)$ have to be met.

Here, two ways of meeting these conditions are considered. The first one is keeping $k_{c,1}$ and $k_{c,2}$ constant. Hence, in the worst case where $\theta_r=\pi$, $k_{c,2}>p_2$ and $k_{c,1}>-p_1$. This way of choosing the feedback gains will be referred to as *constant gain pole placement*.

The second way of making sure $\mathrm{Re}(\lambda)<0$, is to allow $k_{c,2}$ to vary along the trajectory, by choosing it equal to $k_{c,2}=k_{c,20}-p_2\cos(\theta_r)$. Now $\mathrm{Re}(\lambda)<0$, if $k_{c,1}>-p_1$ and $k_{c,20}>0$. It is expected that by using this type of *variable gain pole placement* necessary control actions are smaller than when using constant gains. This is because the variable gain is allowed to be smaller, while still meeting the conditions for $\mathrm{Re}(\lambda)<0$.

It is not straightforward to chose exact values for the feedback gains $k_{c,1}$ and $k_{c,2}$, since there are two requirements to be met. The first requirement is to make the pendulum follow some predefined driving signal $\mathbf{r}(t)$, while the second requirement is to do this with as little control energy as possible. In Sec. II A 2, two possible ways of optimizing the choices for the values of the elements of $\mathbf{K}_c$ are discussed.

#### *2. Optimal control*

In this section, two implementations of optimal control are introduced. Before discussing how to design the controller, it should be clear what is meant by optimal control. The goal of the controller is to keep the experimental chaotic pendulum on a target trajectory, using as little effort as possible. In practice this goal is achieved by finding the minimum of a cost function [17]. This cost function is then defined as the sum of squared deviations from the target trajectory plus the sum of squared control actions needed to keep the system close to the desired trajectory. In linear control theory, this is achieved by model predictive control or linear quadratic control [17].

The most straightforward way to obtain optimal control is by choosing a fixed combination of $k_{c,1}$ and $k_{c,2}$ that results in synchronization of the model equations with data from the experimental pendulum *and* that minimizes a cost function of the form,

$$\mathrm{MSE}=\sum_{i=1}^{N}\frac{1}{N_c}\left(\frac{\delta\omega}{\sigma_\omega}\right)_i^2+\frac{1}{N_c}\left(\frac{\delta\theta}{\sigma_\theta}\right)_i^2+\frac{1}{N_c}\left(\frac{k_{c,1}\delta\omega+k_{c,2}\delta\theta}{\sigma_u}\right)_i^2 =\mathrm{MSE}_\omega+\mathrm{MSE}_\theta+\mathrm{MSE}_u \quad (10)$$

as well, i.e., *constant gain optimal control*. Here MSE is the mean-square error per drive cycle, $N_c$ is the number of drive cycles, and $N$ is the number of discrete time steps at which the control output is evaluated. The deviations from the target trajectory ($\delta\theta$ and $\delta\omega$) are normalized by dividing them by the standard deviations of $\theta$ and $\omega$. The control action ($k_{c,1}\delta\omega+k_{c,2}\delta\theta$) is normalized by dividing it by the standard deviation of the drive term. The standard deviations are determined from time series of the uncontrolled pendulum and are thus a measure for the size of the pendulum's attractor.

Instead of using a fixed combination of feedback gains, model predictive control (MPC) uses target state dependent values of the elements of $\mathbf{K}_c$. This is advantageous since the local stability of the target trajectory can now be used to keep the control actions as small as possible.

When the control of chaotic systems is approached in the drive-response way, cf. Eqs. (1) and (2), this results in a full state feedback algorithm through the linearization of the coupling function $\mathbf{E}$. When using MPC, no coupling is assumed and only the dynamics transverse the target trajectory are considered. These dynamics are captured by the following description:

$$\dot{\mathbf{e}}(t)=\mathbf{DF}_r(\mathbf{r},t)\mathbf{e}(t)+\mathbf{B}u(t), \quad (11)$$

where $u$ is a scalar control input, and $\mathbf{B}=[1\,0\,0]^T$, which determines in which of the ODE's of Eq. (5) the control action takes effect. When only the deviations of the angular velocity and of the angular displacement from the target trajectory are considered, Eq. (11) becomes

$$\dot{\mathbf{e}}(t)=\begin{pmatrix}-p_1 & -p_2\cos(\theta_r(t))\\ 1 & 0\end{pmatrix}\cdot\mathbf{e}(t)+\begin{pmatrix}1\\0\end{pmatrix}\cdot u(t). \quad (12)$$

The goal of MPC is, given an initial deviation $\mathbf{e}_0$ at time $t_0$, to find $u(t_0)\cdots u(t_0+T)$ that minimizes the weighted sum of the squared future deviations from the target trajectory and of the total control energy used within a certain prediction horizon $T$. For that purpose, the following cost function:

$$V=\int_{t_0}^{t_{0+T}}[\mathbf{e}(t)^T\mathbf{Q}\mathbf{e}(t)+\mathbf{B}^Tu(t)\mathbf{R}\mathbf{B}u(t)]dt, \quad (13)$$

is minimized by choosing $u(t_0)\cdots u(t_0+T)$. Matrices $\mathbf{Q}$ and $\mathbf{R}$ are diagonal weighting matrices that are used to tune the controller. These matrices are chosen in such a way, that the cost function becomes equal to $N_c$ times MSE, which will be called the sum of squared errors (SSE). Here $N_c$ is

the number of drive cycles over which the cost function was evaluated. Matrix $\mathbf{R}$ will then have $1/\sigma_u^2$ on its diagonal, and $\mathbf{Q}=\mathrm{diag}(1/\sigma_\omega^2,1/\sigma_\theta^2)$.

When MPC is used to control the experimental pendulum, the equations have to be written in discrete time, since measurements of the pendulum's state are not continuously available. Using a first-order approximation [6], Eq. (12) can be written as

$$\mathbf{e}_{n+1}=\mathbf{A}_n\cdot\mathbf{e}_n+\mathbf{B}\cdot u_n, \quad \text{with}$$

$$\mathbf{A}_\varphi=\begin{pmatrix}1-p_1\cdot\Delta t & -p_2\cos(\theta_r(t_n))\cdot\Delta t\\ 1\cdot\Delta t & 1\end{pmatrix} \quad \text{and}$$

$$\mathbf{B}=\begin{pmatrix}\Delta t\\ 0\end{pmatrix}. \tag{14}$$

This approximation is valid if the sample time ($\Delta t$) is sufficiently small. The discrete version of the cost function of Eq. (13) can now be written as a matrix multiplication,

$$V(\mathbf{U})=\mathbf{X}^T\mathbf{Q}\mathbf{X}+\mathbf{U}^T\mathbf{R}\mathbf{U}, \tag{15}$$

where $\mathbf{X}=[\mathbf{e}_{n+1}^T\mathbf{e}_{n+2}^T\cdots\mathbf{e}_{n+N}^T]^T$ is a column vector containing the future deviations from the target trajectory, and $\mathbf{U}=[u_n\,u_{n+1}\cdots u_{n+N-1}]^T$ is a column vector that contains the current ($u_n$) and all future control actions. $\mathbf{Q}$ and $\mathbf{R}$ are both square weighting matrices. The optimal control actions ($\mathbf{U}_{\mathrm{optimal}}$), corresponding to the minimum of the cost function of Eq. (15), are given by

$$U_{\mathrm{optimal}}=-(\mathbf{R}+\mathbf{B}_0^T\mathbf{Q}\mathbf{B}_0)^{-1}\mathbf{B}_0^T\mathbf{Q}\mathbf{A}_0\mathbf{e}_0=-\mathbf{K}\mathbf{e}_0. \tag{16}$$

These optimal control actions are found by substitution of $\mathbf{X}=\mathbf{A}\cdot\mathbf{e}+\mathbf{B}\cdot\mathbf{U}$ into Eq. (15) and then differentiating the result to $\mathbf{U}$ and solving for the minimum. As can be seen from Eq. (16), the optimum sequence of control actions is given by a feedback control law. This means that MPC provides an optimum way of choosing the feedback matrix $\mathbf{K}$. Matrix $\mathbf{A}_0$ gives the open loop response of the system during the prediction horizon $T=N\cdot\Delta t$. Matrix $\mathbf{B}_0$ gives the influence of the control actions on the system during this prediction horizon. These matrices are defined as follows,

$$\mathbf{A}_0=\begin{pmatrix}\mathbf{A}_n\\ \mathbf{A}_{n+1}\mathbf{A}_n\\ .\\ .\\ .\\ \mathbf{A}_{n+N-1}\ldots\mathbf{A}_n\end{pmatrix}, \quad \mathbf{B}_0=\begin{pmatrix}\mathbf{B} & 0 & 0 & . & \ldots & 0 & 0\\ \mathbf{A}_n\mathbf{B} & \mathbf{B} & 0 & . & \ldots & 0 & 0\\ \mathbf{A}_{n+1}\mathbf{A}_n\mathbf{B} & \mathbf{A}_{n+1}\mathbf{B} & \mathbf{B} & . & \ldots & 0 & 0\\ \mathbf{A}_{n+2}\mathbf{A}_{n+1}\mathbf{A}_n\mathbf{B} & \mathbf{A}_{n+2}\mathbf{A}_{n+1}\mathbf{B} & \mathbf{A}_{n+2}\mathbf{B} & \mathbf{B} & \ldots & 0 & 0\\ . & . & . & . & \ldots & 0 & 0\\ . & . & . & . & \ldots & \mathbf{B} & 0\\ \mathbf{A}_{n+N-1}\ldots\mathbf{A}_n\mathbf{B} & . & . & . & \ldots & \mathbf{A}_{n+N-1}\mathbf{B} & \mathbf{B}\end{pmatrix}. \tag{17}$$

In practice, only the first control action of the optimum sequence ($u_n$) is implemented; when time advances, Eq. (16) is reevaluated to yield the new control action, etc. It is important to notice that these optimal control actions (feedback gains) can be determined off line, if the target trajectory is known.

There are now three adjustable parameters, i.e., the weighting matrices $\mathbf{Q}$ and $\mathbf{R}$, and the prediction horizon $T$ (or $N=T/\Delta t$), to tune the controller to give optimum performance, i.e., to have a minimum value for the mean-square error per drive cycle. This tuning process is still a matter of trial and error.

### B. Observer design

The four ways of controller implementation mentioned in the previous section, i.e., constant and variable gain pole placement, and constant gain optimal control and MPC, all rely on knowledge of the full state of the dynamical system. However, the full state of the experimental pendulum [8,9] cannot be measured. This means it has to be estimated based on only one measured variable, the angular displacement $\theta(t)$. One way of estimating the angular velocity is by differentiation of $\theta(t)$. However any noise and/or measurement error present in $\theta(t)$ is amplified by differentiation. Instead of differentiating the measured angular displacement, an *observer* will be used to estimate the pendulum's full state.

As mentioned in Sec. I an observer is a model that is synchronized with the experimental system. If the observer is successfully synchronized, it's state is an estimate for the experimental system's full state. In this case the set of ODE's given in Eq. (5) is used as the observer model. The difference between the observer's state and the state of the experimental pendulum can be described by

$$\dot{\mathbf{e}}(t)=\left[\begin{pmatrix}-p_2 & -p_2\cos(\theta(t))\\ 1 & 0\end{pmatrix}-\begin{pmatrix}0 & k_{\mathrm{obs.1}}\\ 0 & k_{\mathrm{obs.2}}\end{pmatrix}\right]\cdot\mathbf{e}(t), \tag{18}$$

when the observer is driven by the experimental system, specifically the measured values of $\theta(t)$. The values for both observer gains $k_{\mathrm{obs,1}}$ and $k_{\mathrm{obs,2}}$ should be chosen in such a way that synchronization between the observer and the experimental pendulum is successful, i.e., the difference between the measured angular displacement, $\theta(t)$ and the angular displacement predicted by the observer, becomes small. The constant gain pole-placement technique is used to get an initial estimate for the observer gains $k_{\mathrm{obs,1}}$ and $k_{\mathrm{obs,2}}$.

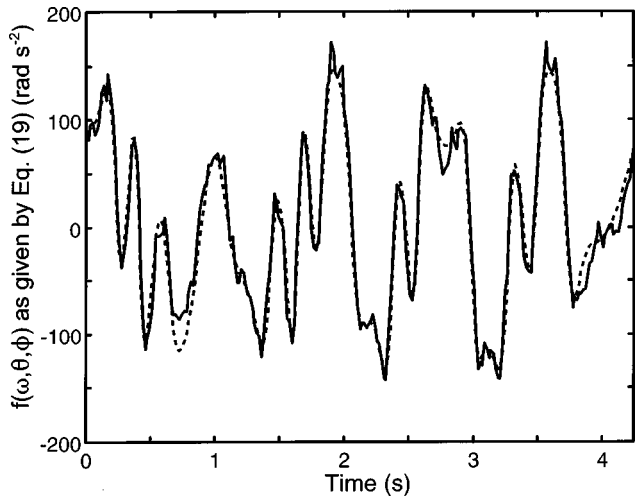


FIG. 2. Result of the least-squares-fit procedure to estimate the unknown parameters of the pendulum model [Eq. (19)]. The solid line shows the measured data that was obtained by differentiating the measured angular displacement twice according to Eq. (20). The broken line shows the model fit with parameter values $p_1=0.74 \pm 0.001\ \mathrm{s}^{-1}$, $p_2=78.26\pm 0.26\ \mathrm{rad\,s}^{-2}$, and $p_3=66.18 \pm 0.21\ \mathrm{rad\,s}^{-2}$. The pendulum model will be used as an observer, to estimate the pendulum's full state from measurements of only the angular displacement $\theta(t)$.

## III. RESULTS

The pendulum used is a type *EM*-50 chaotic pendulum produced by the Daedalon Corporation (Salem, MA, USA) [9]. The pendulum arm itself is connected to an axis with an optical encoder wheel and a ring magnet attached to it. Four electromagnetic drive coils act as a motor that generates a torque acting on the ring magnet. The optical encoder wheel contains a large number of slots that can optically be detected so that the angle ($\theta$) of the pendulum can be measured with a resolution of 4000 positions ($=2\pi$ rad). An 80 486-based computer with a digital-to-analog converter generates a sinusoidal voltage that is transformed to a sinusoidal torque by the pendulum's electronics and driving mechanism. The frequency $f=2\pi/\omega_D$ of this sinusoidal drive voltage is 0.85 Hz. The pendulum's angle is read 50 times per drive cycle, so the sample time $\Delta t=1/50T_c$, where $T_c=1/f$ is the length of a drive cycle in seconds.

### A. Observer design

The design of the observer is split into two steps. In the first step, a model is estimated that describes the pendulum's dynamics. In the second step, the observer feedback gains $k_{\mathrm{obs},1}$ and $k_{\mathrm{obs},2}$ are estimated.

Step 1: determination of observer model. In principle for the observer any type of model is adequate, as long as it is possible to linearize the model along the target trajectory. Black box type of models as neural networks, as well as sets of ordinary differential equations can be used to describe the functional relationship between the current state, the control input, and the future state, the output. There are methods available in literature [21,22] to determine differential equation models from measured data. In this case the set of ordinary differential equations that describes the pendulum's dynamics are known, Eq. (5). The unknown parameters ($p_1$, $p_2$, and $p_3$) were estimated by fitting,

$$\frac{d\omega}{dt}=f(\omega,\theta,\phi)=-p_1\omega-p_2\sin(\theta)+p_3\sin(\phi), \quad (19)$$

to experimental data, using a method similar to that of Baker, Gollub, and Blackburn [21]. The acceleration of the pendulum ($d\omega/dt$) and its angular velocity ($\omega$) are estimated by differentiating the measured angle $\theta(t)$, which is sampled using a sample time $\Delta t$, according to

$$\omega(t)=\frac{\theta(t+\Delta t)-\theta(t-\Delta t)}{2\Delta t},$$

$$\frac{d\omega(t)}{dt}=\frac{\theta(t+\Delta t)-2\theta(t)+\theta(t-\Delta t)}{\Delta t^2}. \quad (20)$$

The drive phase $\phi(t)$ is known and is $\omega_D\cdot t$. Since $d\omega/dt$, $\omega$, $\sin(\theta)$, and $\sin(\phi)$ are all known, parameters $p_1$, $p_2$, and $p_3$ can be estimated by using a linear least-squares-fit procedure. Due to the amplification of noise by differentiating measured data, it is not wise to use $\omega(t)$ and $d\omega/dt$ obtained from Eq. (20) as estimates for the full state during control. However, for the off-line estimation of the unknown parameters, it is wise to use Eq. (20). Figure 2 shows the fitted and measured angular acceleration ($d\omega/dt$), for the given parameter values. The model thus obtained exhibits chaotic behavior and has a Poincaré map similar to the experimental pendulum (see Fig. 3).

Step 2: determination of observer gains. An adequate model for the observer is now available and the observer

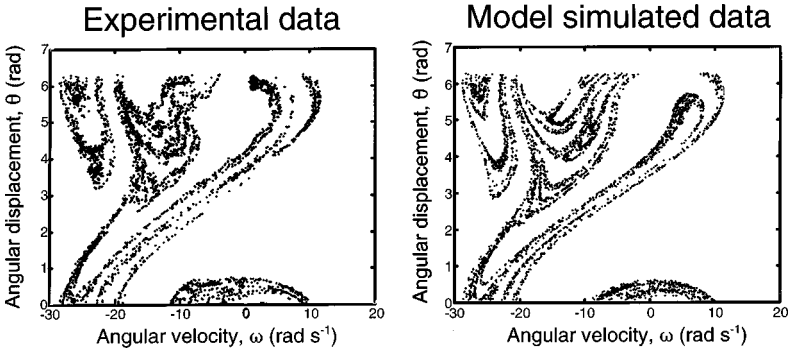


FIG. 3. Poincaré maps of both the experimental pendulum and the model, Eq. (5) with the estimated parameter values. This Poincaré map was constructed by recording the angular velocity ($\omega$) and the angular displacement ($\theta$), each time the drive phase ($\phi$) was equal to a multiple of $2\pi$ rad.

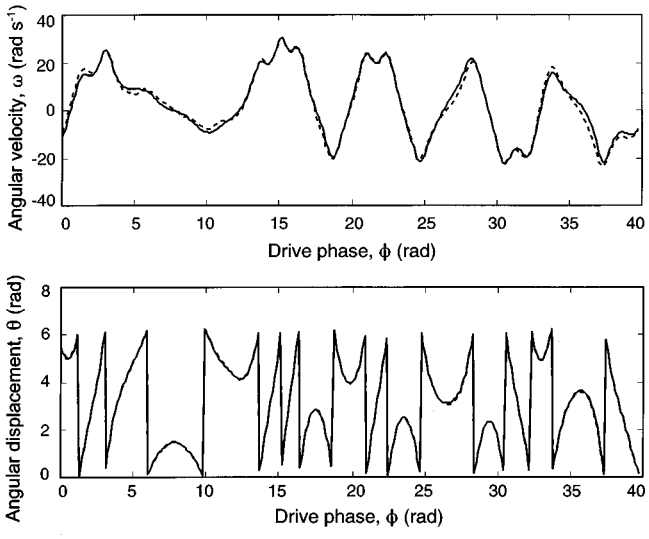


FIG. 4. To determine the optimal observer constants the pendulum model [Eq. (5)] was synchronized with a time series of previously measured angular displacements (solid lines) using feedback control according to Eq. (18). The observer constants were adjusted using a simplex minimization routine, to minimize the sum of squared deviations from the measured data of both the angular displacement and angular velocity predicted by the model. Since the angular velocity of the pendulum could not be measured, it was calculated from the angular displacement according to Eq. (20). The broken lines show the observer's state when the optimal observer constants ($k_{\mathrm{obs},1}=182\,\mathrm{s}^{-2}$, $k_{\mathrm{obs},2}=46\,\mathrm{s}^{-1}$) are used to synchronize the model with the experimental data.

gains can be determined. The observer gains ($k_{\mathrm{obs},1}$ and $k_{\mathrm{obs},2}$) were determined by synchronizing the model [Eq. (5)] with a previously measured time series containing $N$ time steps using the feedback scheme proposed in Eq. (18). The following cost function:

$$V=\sum_{i=1}^{N}\left(\frac{\delta\omega}{\sigma_\omega}\right)_i^R+\left(\frac{\delta\theta}{\sigma_\theta}\right)_i^2+\left(\frac{k_{\mathrm{obs}.1}\delta\theta}{\sigma_u}\right)_i^2+\left(\frac{k_{\mathrm{obs}.2}\delta\theta}{\sigma_\omega}\right)_i^2, \tag{21}$$

was minimized for optimizing the observer. The differences between the pendulum's and observer's state ($\delta\theta$ and $\delta\omega$) were normalized using $\sigma_\omega$, $\sigma_\theta$, and $\sigma_u$, the standard deviations of $\omega(t)$, $\theta(t)$, and the drive signal, respectively. These standard deviations are determined from the data with which the observer is synchronized. Figure 4 shows the observer performance using the optimum values for $k_{\mathrm{obs},1}$ and $k_{\mathrm{obs},2}$. These values were obtained by using a simplex minimization routine.

### B. Full state feedback control

To illustrate the suggested control methods, six different target trajectories were used: (i) AO-1 (aperiodic orbit 1), an arbitrary continuous piece of time series consisting of 40 drive periods, (ii) P-1, a period-1 orbit calculated from the model. (iii) P-2, a period-2 orbit calculated from the model. This calculation was done by locating a close returning point in the Poincaré section (Fig. 3) of the model that was used as a first estimate for a fixed point. Then this estimate was refined by using a simplex minimization that minimized the distance on the Poincaré section between the close returning points. The coordinates of the fixed point thus obtained were used to generate the complete orbit, and (iv) P-3a to P-3c, period-3 periodic orbits extracted from measured data. Again close returning points were located, but now using experimental data.

#### *1. Pole placement*

The experimental pendulum was first synchronized with AO-1 using the *constant gain pole-placement* technique discussed in Sec. II A 1. Three arbitrary combinations of $k_{c,1}$ and $k_{c,2}$ were chosen that satisfy the worst case conditions to keep $\mathrm{Re}(\lambda)<0$. Table I shows the synchronization results

TABLE I. Results of the *constant gain pole-placement* method. Here the experimental pendulum is synchronized with different target trajectories using constant feed back gains. These gains are chosen in such a way that the poles of the controlled system that is linearized along the target trajectory [Eq. (8)], will always have negative real parts. If these real parts are chosen to be sufficiently negative, this always results in successful synchronization. The controller performance is expressed by the MSE per drive cycle, which is the sum of normalized squared deviations from the target trajectory plus the sum of normalized squared control actions, averaged over one drive cycle of the experimental pendulum. Here target trajectory P-3a is best stabilized using this specific combination of feedback constants.

| Target trajectory | Feedback gains | | MSE | Individual contributions to the MSE [Eq. (10)] | | |
|---|---|---|---|---|---|---|
| | $k_{c,1}$ | $k_{c,2}$ | | $\mathrm{MSE}_\omega$ | $\mathrm{MSE}_\theta$ | $\mathrm{MSE}_u$ |
| AO-1 | 48.58 | 78.26 | 2.433 | 0.021 | 0.342 | 2.070 |
| AO-1 | 54.49 | 117.39 | 1.710 | 0.051 | 0.196 | 1.495 |
| AO-1 | 69.31 | 234.78 | 1.347 | 0.018 | 0.080 | 1.249 |
| P-1 | 54.49 | 117.39 | 1.050 | 0.195 | 1.399 | 8.456 |
| P-2 | 54.49 | 117.39 | 5.932 | 0.111 | 0.846 | 4.974 |
| P-3a | 54.49 | 117.39 | 0.417 | 0.003 | 0.014 | 0.401 |
| P-3b | 54.49 | 117.39 | 4.360 | 0.063 | 0.536 | 3.760 |
| P-3c | 54.49 | 117.39 | 1.382 | 0.017 | 0.126 | 1.238 |

TABLE II. Results of the *variable gain pole-placement* method. In contrast to the constant gain pole-placement method (Table I), $k_{c,2}$ is allowed to vary along the target trajectory according to $k_{c,2}=k_{c,20}-p_2\cos(\theta_r(t))$. Here the values for $k_{c,1}$ and $k_{c,20}$ are chosen in such a way that the poles of the controlled system, which is linearized along the target trajectories [Eq. (8)], have negative real parts. If these real parts are sufficiently negative, this will result in synchronization. Clearly for the first two choices of the feedback gains, synchronization fails as is indicated by the large values for the MSE per drive cycle.

| Target trajectory | Feedback gains | | MSE | Individual contributions to the MSE [Eq. (10)] | | |
|---|---|---|---|---|---|---|
| | $k_{c,1}$ | $k_{c,20}$ | | $\mathrm{MSE}_\omega$ | $\mathrm{MSE}_\theta$ | $\mathrm{MSE}_u$ |
| AO-1 | 0.75 | 0.141 | 102.697 | 41.379 | 43.036 | 18.280 |
| AO-1 | 7.50 | 4.254 | 44.411 | 11.215 | 19.441 | 13.721 |
| AO-1 | 37.50 | 91.44 | 1.236 | 0.015 | 0.171 | 1.050 |
| AO-1 | 75.0 | 358.63 | 1.443 | 0.016 | 0.037 | 1.390 |
| P-1 | 37.50 | 91.44 | 8.398 | 0.125 | 1.306 | 6.967 |
| P-2 | 37.50 | 91.44 | 4.956 | 0.064 | 0.623 | 4.269 |
| P-3a | 37.50 | 91.44 | 0.211 | 0.002 | 0.074 | 0.196 |
| P-3b | 37.50 | 91.44 | 4.602 | 0.054 | 0.589 | 3.959 |
| P-3c | 37.50 | 91.44 | 0.373 | 0.003 | 0.024 | 0.346 |

where MSE, Eq. (10), and its three components are shown as an indication of controller performance. One of the combinations of feedback gains was used to synchronize the experimental pendulum with the other target trajectories. Using this specific choice of gains ($k_{c,1}=54.49$ and $k_{c,2}=117.39$), P-3a is best stabilized (MSE$=0.417$).

The *variable gain pole-placement* technique was used to synchronize the pendulum with AO-1 (see Table II). The combination of $k_{c,1}$ and $k_{c,20}$ that gave the smallest value for MSE ($=1.236$) was used to synchronize the pendulum with the other target trajectories. Again P-3a is best stabilized, MSE is almost twice as low as when using *constant gain pole placement* (see Fig. 5).

### *2. Optimal control*

When inspecting the results presented in Tables I and II, it is not obvious which values to choose for the feedback gains in order to obtain a minimal MSE. When a certain combination of feedback gains results in a small MSE for one target trajectory, it does not necessarily result in a small MSE for another target trajectory. When using optimal controllers, this is dealt with since optimal controller design is based on minimizing the sum of squared errors (SSE); that is the product of $N_c$ and MSE.

Synchronization is more successful, i.e., smaller values for MSE, for all target trajectories (Table III), when using *constant gain optimal control*, compared to the results that

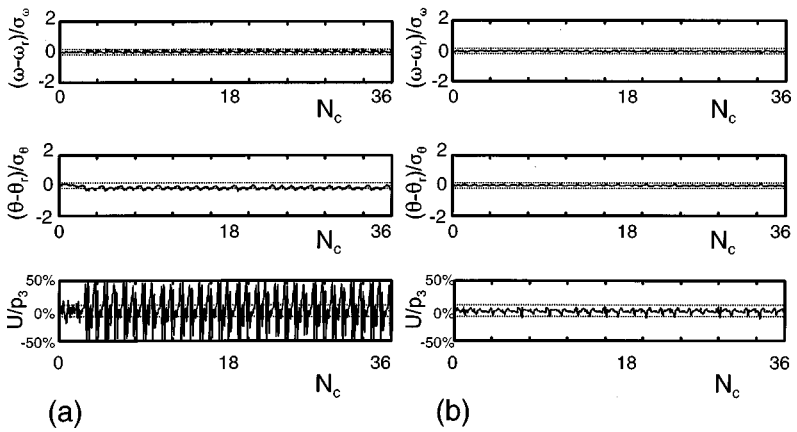


FIG. 5. Results of the *constant gain optimal-control* technique. The figures show the normalized deviations from the target trajectories, and the size of the control actions relative to the drive amplitude ($p_3$) of the pendulum [Eq. (5)]. The broken lines indicate levels corresponding to $\pm 10\%$ of the standard deviation ($\sigma_\theta$ or $\sigma_\omega$) of the uncontrolled, chaotic dynamics of both the angular velocity ($\omega$) and the angular displacement ($\theta$). (a) Although the experimental pendulum follows target trajectory P-1 well, a considerable control input is needed. Most of the time control actions exceeding 10% of the drive amplitude are needed. The broken lines indicate the $\pm 10\%$ boundary. The MSE [Eq. (10)], which is indicative for the controller performance, has a value of 7.093. The largest contribution to this value is due to the control actions, 5.582 ($=78.7\%$). (b) The experimental pendulum synchronizes very well with target trajectory P3-b. The control actions needed stay well within the $\pm 10\%$ boundary. The MSE in this case is 0.156 and the contribution of the control actions to MSE equals 0.075 ($=48.1\%$).

TABLE III. Results of the *constant gain optimal-control* method. The optimal feedback gains were obtained by synchronizing the model Eq. (5) with the different target trajectories with simultaneous minimization of the MSE per drive cycle using a simplex minimization routine (MSE optimization). The optimal feedback gains thus obtained were then used to synchronize the experimental pendulum with the different target trajectories (MSE measurement). Clearly target trajectories P-3a and P-3b are best stabilized using only very little control effort.

| Target trajectory | Feedback gains | | MSE | | Individual contributions to the measured MSE [Eq. (10)] | | |
|---|---|---|---|---|---|---|---|
| | $k_{c,1}$ | $k_{c,2}$ | Optimization | Measurement | $MSE_\omega$ | $MSE_\theta$ | $MSE_u$ |
| AO-1 | 36.28 | 332.97 | 13.131 | 0.940 | 0.025 | 0.018 | 0.897 |
| P-1 | 19.95 | 30.19 | 0.010 | 7.093 | 0.172 | 1.339 | 5.582 |
| P-2 | 5.91 | 80.68 | 0.017 | 1.742 | 0.151 | 0.125 | 1.466 |
| P-3a | 7.28 | 41.56 | 2.363 | 0.156 | 0.014 | 0.024 | 0.118 |
| P-3b | 3.26 | 34.17 | 1.703 | 0.156 | 0.040 | 0.041 | 0.075 |
| P-3c | 10.41 | 101.94 | 4.543 | 0.183 | 0.012 | 0.010 | 0.161 |

were obtained using the pole-placement method. Another remarkable result is that the MSE's of P-1 and P-2 are the largest in the experiment, and the smallest in the simulation that was done to estimate the gains. This result is best explained by considering the origin of the P-1 and P-2 orbits. Both orbits were calculated using the model, whereas the other orbits are all determined from experimental data.

Although *constant gain optimal control* has a better performance (smaller MSE's) than both methods based on pole placement, model predictive control results in even better performance. This is expected since with MPC the gains vary along the target trajectory, taking advantage of the local stability of the target trajectory.

When using MPC the weighting matrices **Q** and **R** as well as the length of the prediction horizon $T$ have to be chosen. In this paper **Q** and **R** are chosen in such a way that the cost function given in Eq. (15) becomes the same as $N_c \cdot \mathrm{MSE}$ when the weights ($W_\omega$, $W_\theta$, and $W_u$) on the individual contributions to MSE ($MSE_\omega$, $MSE_\theta$, and $MSE_u$) are set to unity. Here *Nc* is the number of drive cycles over which Eq. (15) is evaluated and MSE is defined by Eq. (10).

Choosing the optimal tuning parameters ($T$, $W_\omega$, $W_\theta$, and $W_u$) is still a matter of trial and error. However, this can be automated by simulation of the controlled nonlinear process and tuning of the weight parameters until the minimum in the MSE is reached. Here this automation process is not implemented, rather just a number of possible combinations are screened for the AO-1 as target trajectory. Then after reducing the number of possible combinations, the other target trajectories were stabilized as well.

The AO-1 was chosen as the target trajectory for the purpose of screening a number of possible prediction horizon lengths. The number of time steps in the prediction horizon ($N$) was chosen to be 5, 10, 25, and 50 time steps, which is equivalent to 0.1, 0.2, 0.5, and 1 times the driving period of the pendulum ($T_c$). Three fixed combinations for the weights were used, i.e., $[W_\omega W_\theta W_u]=[1\ 1\ 1]$ that is equivalent to minimizing MSE, and $[W_\omega W_\theta W_u]=[1\ 5\ 5]$, or [1 10 10], which puts a larger penalty on differences between the measured and target angle and the magnitude of the control actions.

The twelve resulting MSE's are shown in Table IV. As is

TABLE IV. Results of the model predictive control method. The MSE's per drive cycle are shown for the synchronization of the experimental pendulum with AO-1. The feedback gains that were used are calculated by minimizing the SSE over a certain prediction horizon. This SSE [Eq. (15)] consists of three contributions, i.e., the squared normalized deviations of the angular velocity, the squared normalized deviations of the angular displacement, and the squared normalized control actions. A weight of [1 1 1] means that each contribution to the SSE is weighted equally in the calculation of the optimal feedback gains. A prediction horizon of 5 time steps is too small for successful synchronization. The most successful synchronization (smallest MSE's) is obtained when a prediction horizon of 25 time steps, or half a drive cycle, is used. Putting more weight on the contributions of the control actions and the angular displacement to the SSE does not result in improved controller performance.

| Prediction horizon (time steps) | Weights on the individual contributions to SSE | | |
|---|---|---|---|
| | [1 1 1] | [1 5 5] | [1 10 10] |
| 5 | 51.966 | 92.187 | 76.086 |
| 10 | 2.168 | 4.372 | 14.813 |
| 25 | 0.418 | 0.436 | 0.428 |
| 50 | 0.874 | 0.861 | 0.753 |

TABLE V. Results using MPC. In this table the results are shown of using MPC to synchronize the experimental pendulum with the different target trajectories. The length of the prediction horizon was taken as 10 time steps. The most striking result of using MPC is that the experimental pendulum is synchronized well with P-1 and P-2, opposed to the results presented in Tables I, II, and III. Again increasing the weight on the contribution of the control actions to the optimization criterion (SSE), does not result in smaller control effort needed to stabilize the pendulum; see also Table IV.

| Target trajectory | Weights on the individual contributions to SSE | | | | | |
|---|---|---|---|---|---|---|
| | [1 1 1] | | [1 5 5] | | [1 10 10] | |
| | MSE | $MSE_u$ | MSE | $MSE_u$ | MSE | $MSE_u$ |
| AO-1 | 2.168 | 0.681 | 4.372 | 0.927 | 14.813 | 2.504 |
| P-1 | 1.512 | 0.346 | 1.568 | 0.361 | 2.620 | 0.516 |
| P-2 | 1.190 | 0.272 | 1.290 | 0.203 | 1.210 | 0.181 |
| P-3a | 0.204 | 0.074 | 1.089 | 0.252 | 1.657 | 0.390 |
| P-3b | 1.549 | 0.267 | 0.290 | 0.039 | 0.302 | 0.045 |
| P-3c | 0.237 | 0.079 | 0.399 | 0.100 | 0.734 | 0.164 |

clear from Table IV the optimal choice is taking the number of time steps in the prediction horizon equal to $N=25$ and the weights $[W_\omega W_\theta W_u]=[1\ 1\ 1]$. A prediction horizon of $N=5$ is too small to synchronize the experimental pendulum with the target trajectory. However, when $N=10$, the pendulum synchronizes with AO-1.

A prediction horizon of $N=10$ is chosen when synchronizing the experimental pendulum with the other target trajectories. This choice was made, since $N$ is large enough to yield successful synchronization, but is still small enough to avoid large computation times. The weights on the individual contributions of the MSE ($W_\omega$, $W_\theta$, and $W_u$), were chosen the same as when synchronizing AO-1. The resulting MSE's as well as the contribution of the control actions to MSE are reported in Table V.

Increasing the penalties on the $MSE_\theta$ an $MSE_u$ does not result in smaller MSE's for all target trajectories but P-3b. Furthermore, the effect on the contribution of the control actions to the MSE of an increased penalty on $MSE_u$, is not clear. In most cases $MSE_u$ grows with increasing penalty, however, not when P-2 and P-3b are the target trajectories. This result indicates that by changing the penalty (or weight) on the different contributions to MSE, controller performance can be enhanced in some cases.

The *constant gain optimal control* method has the best performance, i.e., smallest MSE's for all target trajectories but P-1 and P-2. In these cases model predictive control clearly has the better performance. However, closer inspection of the results in Table IV suggest that MPC will outperform the constant gain optimal control method, when the prediction horizon is chosen to be $N=25$. The MSE, when AO-1 is the target trajectory, is more than halved when using MPC and $N=25$ (MSE=0.418, Table IV) compared to the constant gain case (MSE=0.940, Table III).

## IV. CONCLUSIONS

In this paper a general procedure has been outlined to control chaotic systems using linear control methods. In contrast with other chaos control procedures [13–15,19], the procedure outlined in this paper automatically results in a choice for the feedback gains that gives optimum performance, i.e., minimum fluctuations around the desired trajectory, using minimum control actions. The procedure consists of four steps. In the first step, a model of the system is built. In the second step target trajectories are defined, which may be AO's corresponding to previously observed trajectories, or UPO's. In the third step, the optimal feedback constants along the target trajectories are determined using MPC. Finally, in the fourth step, the controller is implemented in the experimental setup. This approach shows that linear control methods, specifically model predictive control, are well applicable to control nonlinear chaotic dynamical systems. The approach is illustrated by the successful control of an experimental chaotic system, i.e., a driven damped pendulum.

## ACKNOWLEDGMENT

The investigations were supported in part by the Netherlands Foundation for Chemical Research (SON) as part of the SON Program ''Young Chemists'' with financial aid from the Netherlands Organization for Scientific Research (NWO).

[1] L. M. Pecora and T. L. Carroll, Phys. Rev. Lett. **64**, 821 (1990).
[2] K. M. Cuomo and A. V. Oppenheim, Phys. Rev. Lett. **71**, 65 (1993).
[3] N. F. Rulkov, Chaos **6**, 262 (1996).
[4] E. R. Hunt, Phys. Rev. Lett. **67**, 1953 (1991).
[5] F. C. Moon, M. A. Johnson, and W. T. Holmes, Int. J. Bifurcation Chaos Appl. Sci. Eng. **6**, 337 (1996).
[6] B. Hübinger, R. Doerner, H. Heng, and W. Markienssen, Int. J. Bifurcation Chaos Appl. Sci. Eng. **4**, 773 (1994).
[7] D. J. Christini, J. J. Collins, and P. S. Linsay, Phys. Rev. E **54**, 4824 (1996).

[8] R. Bakker, J. C. Schouten, F. Takens, and C. M. van den Bleek, Phys. Rev. E **54**, 3545 (1996).
[9] R. J. de Korte, J. C. Schouten, and C. M. van den Bleek, Phys. Rev. E **52**, 3358 (1995).
[10] M. Vasudevan, C. E. A. Finney, K. Nguyen, N. A. Goor, D. D. Burns, and C. S. Daw, in *Proceedings of the 13th International Conference on Fluidized Bed Combustion, Orlando, Florida, 1995*, edited by K. J. Heinschel (American Society of Mechanical Engineers, New York, 1995), p. 1006.
[11] S. Kaart, J. C. Schouten, and C. M. van den Bleek, in *Proceedings of the 2nd International Symposium Catalysis in Multiphase Reactors, Toulouse, France, 1998*, edited by H. Delmas (Progep, Toulouse, 1998), p. 237.
[12] S. Kaart, J. C. Schouten, and C. M. van den Bleek, in *Fluidization IX*, edited by L. S. Fan and T. M. Knowlton (Engineering Foundation, New York, 1998), p. 621.
[13] G. Chen and X. Dong, Int. J. Bifurcation Chaos Appl. Sci. Eng. **3**, 1363 (1996).
[14] T. Shinbrot, Adv. Phys. **44**, 73 (1995).
[15] T. Kapitaniak, *Controlling Chaos—Theoretical and Practical Methods in Nonlinear Dynamics* (Academic, London, 1996).
[16] K. Glass, M. Adachi, and A. Mees, Int. J. Bifurcation Chaos Appl. Sci. Eng. **6**, 1330 (1996).
[17] B. Friedland, *Control System Design—An Introduction to State-Space Methods* (McGraw-Hill, New York, 1986).
[18] H. Kwakernaak and R. Sivan, *Linear Optimal Control Systems* (Wiley-Interscience, New York, 1972).
[19] R. Brown and N. F. Rulkov, Chaos **7**, 395 (1997).
[20] P. Ashwin, J. Buescu, and I. Stewart, Phys. Lett. A **193**, 126 (1994).
[21] G. L. Baker, J. P. Gollub, and J. A. Blackburn, Chaos **6**, 528 (1996).
[22] C. Letellier, L. Le Sceller, G. Gouesbet, F. Lusseyran, A. Kemam, and B. Izrar, AIChE. J. **43**, 2194 (1997).